Overexpression of *STAY-GREEN* in dark-incubated leaves prompts the formation of transitional chromoplast-like plastids

Hui Zheng [a], Salvador Torres-Montilla [b], Xingqi Huang [a], Manuel Rodríguez-Concepción [b,*], Shan Lu [a,*]

[a] Stake Key Laboratory of Pharmaceutical Biotechnology, School of Life Sciences, Nanjing University, Nanjing 210023, China.

[b] Institute for Plant Molecular and Cell Biology (IBMCP), CSIC-Universitat Politècnica de València, Valencia 46022, Spain.

***Corresponding authors:**

manuelrc@ibmcp.upv.es (M.R.-C.); and shanlu@nju.edu.cn (S.L.).

The authors responsible for distribution of materials integral to the findings presented in this article in accordance with the policy described in the Instructions for Authors (https://academic.oup.com/plphys/pages/General-Instructions) are: Manuel Rodríguez-Concepción (manuelrc@ibmcp.upv.es) and Shan Lu (shanlu@nju.edu.cn).

Running head: *STAY-GREEN* facilitates plastid differentiation

Abstract

The transition of chloroplasts during fruit ripening and leaf senescence into chromoplasts and gerontoplasts involves a shared process of chlorophyll breakdown and chloroplast deterioration. Chlorophyll removal is carried out by several enzymes. Among them, STAY-GREEN (SGR) is a Mg dechelatase that catalyzes the first step of chlorophyll degradation. Tomato *green-flesh* (*gf*) and pepper *chlorophyll retainer* (*cl*) mutants are SGR loss-of-function mutants and were proven to maintain a high level of thylakoid structures during chromoplast development in fruit ripening. Here, by overexpressing *SGR* in non-illuminated *Nicotiana benthamiana* leaves, we forward demonstrate that SGR itself has the ability to cue the onset of chloroplast deterioration, strikingly resulting in the formation of orange leaf sectors containing plastids with carotenoid-bearing structures despite carotenoid production is not induced. Metabolic, microscopy, and transcriptomic analyses further suggested an onset of chloroplast senescence, indicating a possible transitional plastid stage in SGR regions. Our work hence demonstrates a remarkable ability of plant plastids to adapt their ultrastructure to accommodate the precise metabolic composition in various developmental and environmental contexts.

Keywords

Carotenoid; chlorophyll breakdown; chloroplast deterioration; chromoplast; plastid differentiation; STAY-GREEN (SGR)

Introduction

Plastids are plant-specific semi-autonomous organelles that carry out a wide diversity of essential physiological processes under a tightly coordinated regulation between the nucleic and the plastidial genomes (Sadali et al., 2019). Different from algae and mosses that have chloroplast as the only form of plastids, higher plants have evolved different forms of plastids with various structures and functions, of which the biogenesis, distribution, and transition are largely determined by developmental cues (Solymosi et al., 2018). Among these forms, chloroplasts in green tissues, especially the leaves, are best characterized for photosynthesis, as well as other pivotal metabolic activities such as the biosynthesis of amino acids (*e.g.*, phenylalanine, tyrosine, tryptophan, *etc.*) and terpenoids (*e.g.*, carotenoids, monoterpenes, gibberellins, abscisic acid, *etc.*) (Lancien et al., 2007; Rolland et al., 2012; Nisar et al., 2015; Sierra et al., 2023). Besides chloroplasts, chromoplasts generally localized in flowers, fruits, and storage organs such as carrot roots have also been extensively studied for their capabilities in the biosynthesis and accumulation of carotenoids (Wen et al., 2020; Liu et al., 2024; Wang et al., 2024). In other developmental contexts, plastids take on different forms, such as the color-less leucoplasts that accumulate starch (amyloplasts), protein (proteinoplasts) and oil (elaioplasts), and gerontoplasts where the recycling of nutrients from senescent leaves to other developing organs occurs (Sierra et al., 2023).

All forms of plastids are initially developed from the non-pigmented proplastids, and can be transformed during organ/tissue development. For example, the transformation from etioplasts to chloroplasts during de-etiolation is one of the most critical developmental events in germinating seedlings, and the transformations from chloroplasts to chromoplasts and gerontoplasts account for the distinct color change during the ripening of fruits and the senescence of leaves, respectively (Li and Yuan, 2013; Sadali et al., 2019). The studies of these transformations have identified a few transitional plastid types, which allow for a more nuanced interpretation of essential developmental scenarios (Solymosi et al., 2018). Specifically, the etiochloroplasts in de-etiolating cotyledons are the transitional form between etioplasts and chloroplasts, contain both prolamellar bodies (PLBs, of etioplasts) and grana (of chloroplasts), and are regarded as a checkpoint that modulates the switch from heterotroph to autotroph stages during germination (Pfannschmidt, 2010). The chromochloroplasts observed in

regreening ripe pumpkin fruits, carrot roots, and lemon fruits contain both grana (of chloroplasts) and plastoglobules (of chromoplasts), indicating the initiation of the switch from active photosynthesis to storage (Ljubesic et al., 1991; Roca et al., 2006; Solymosi et al., 2018).

Along with de-etiolation and ripening, senescence is another critical developmental event, during which the reallocation of nutrients from one pool (*e.g.*, senescent leaves) to another (*e.g.*, seeds) occurs. Both the chloroplast-to-gerontoplast and the chloroplast-to-chromoplast transformations share the characteristic decrease in the contents of chlorophylls, which is generally associated with the disassembly of pigment-protein complexes in the thylakoid membrane (Hortensteiner, 2006; Krupinska, 2007). Chlorophyll breakdown may play a similar role in these two plastid differentiation routes. The breakdown of chlorophylls during senescence is catalyzed by a series of enzymes (Figure 1A). In brief, the magnesium ion (Mg^{2+}) is initially removed from the tetrapyrrole ring of chlorophyll *a* (Chl *a*) by the dechelatase STAY-GREEN (SGR) to produce pheophytin *a* (Pheo *a*), of which the phytyl side chain is subsequently removed by pheophytinase (PPH) to produce pheophorbide *a* (Pheide *a*). Pheide *a* is further converted to colorless primary fluorescent chlorophyll catabolite (*p*FCC) by Pheide *a* oxygenase (PAO) and the red chlorophyll catabolite reductase (RCCR). The final nonfluorescent chlorophyll catabolites (NCCs) are stored in the vacuole (Yang et al., 2019).

Besides catalyzing the dechelation of Mg^{2+} as the first committed step of chlorophyll degradation, SGR also regulates the expression of genes encoding other chlorophyll degradation enzymes such as PPH, PAO, and Non-Yellow Coloring 1 (NYC1), which catalyzes the conversion from Chl *b* to Chl *a* (Figure 1A) (Sato et al., 2018; Ono et al., 2019). SGR is implicated in the destabilization of the light-harvesting complex (LHC) proteins and the dismantling of chlorophyll-protein (CP) complexes (Jiang et al., 2007; Park et al., 2007; Sakuraba et al., 2012; Shimoda et al., 2016; Ying et al., 2021) and it has been shown to directly interact with phytoene synthase (PSY), the rate-limiting entry enzyme for carotenoid synthesis, suggesting that SGR might contribute to coordinate chlorophyll degradation and carotenoid synthesis (Luo et al., 2013). However, the involvement of SGR in the transformation from chlorophyll-

bearing chloroplasts to carotenoid-dominant chromoplasts or gerontoplasts has not been well elucidated.

Here, we show that the agroinfiltration of constructs to produce SGR artificially in dark-incubated *Nicotiana benthamiana* leaves not only caused the degradation of chlorophylls but also resulted in the formation of orange leaf sectors containing plastids with carotenoid-bearing structures similar to those found in natural chromoplasts despite carotenoid production is not induced (Figure 1B). This striking phenotype could not be phenocopied by expressing other genes involved in chlorophyll degradation. Transcriptomic and morphological results suggested an onset of chloroplast senescence, indicating a possible transitional plastid stage in SGR regions between chromoplasts and gerontoplasts. In conclusion, our results provide additional insights supporting the postulation that metabolic alterations are major drivers in the development of plastid ultrastructure.

Results

Overexpression of *SGR* resulted in an orange-leaf phenotype in darkness

One of the most distinct changes during both etioplast-to-chloroplast and chloroplast-to-chromoplast transitions is in the contents of chlorophylls. To assess the involvement of chlorophyll metabolism in leaf plastid conversion, we individually overexpressed *SGR*, *PPH*, *PAO*, as well as the gene for chlorophyllase (*CLH1*), which is known to remove the phytyl side chain from chlorophylls, in leaves of *N. benthamiana* by infiltration, with the enhanced yellow fluorescent protein (EYFP) as a control (Figures 1 and 2). After a 3-d post-agroinfiltration growth in the dark (covered with aluminum foil), the *SGR*-overexpressing leaf region (SGR-region) developed a conspicuous orange color (Figures 1B and 2A). This change was characterized by a significant decline in chlorophyll contents and the retention of almost all carotenoids, resulting in a highest carotenoid-to-chlorophyll ratio among all the transfected samples (Figure 2A). Consistent with this, different accumulations of chlorophyll breakdown products were identified from our quantification. Whereas the *SGR*-overexpressing leaves accumulate small amounts of Pheo *a* and Pheide *a*, both *CLH1*- and *PPH*-overexpressing leaves showed significant accumulation of Chlide *a* (Supplementary

Figure S1). Besides *PPH* and *CLH1*, the overexpression of other representative genes involved in different steps of chlorophyll degradation, including *CLD1* for another chlorophyll dephytylase located in the chloroplast and *NYC1* and *NOL* for the reduction of Chl *b*, could not phenocopy the striking color change of the *SGR*-overexpression leaves either, suggesting a unique role of Mg dechelation catalyzed by SGR in driving this phenotypic transition (Figure 2A and Supplemental Figure S2). When the infiltrated leaves were grown in the light, the SGR-regions exhibited a bleached and necrotic appearance instead of the orange phenotype observed in the dark (Figure 2B). To investigate the effect of light on the development of the SGR-dependent orange leaf phenotype, we treated the dark-grown *SGR*-overexpressing leaves by exposing them to light for one additional day. The results showed that the orange sectors of the leaf bleached after light exposure (Supplemental Figure S3A). However, when we incubated the light-grown *SGR*-overexpressing leaves in darkness for one additional day, the orange phenotype partially recovered (Supplemental Figure S3A). Trypan blue staining revealed more dead cells in the SGR-regions when the leaf was grown in the light than in the dark, irrespective of the initial grown condition being in the light or dark. This observation indicates that *SGR* expression induces photodamage, while darkness can prevent and save the light-damaged phenotype (Supplemental Figure S3B) (Park et al., 2007; Jiang et al., 2011). Pigment analysis of the leaf regions revealed that SGR induced the most pronounced decrease in chlorophyll contents in both light and dark conditions (Figure 2). However, carotenoid content declined with chlorophyll loss only in the light (Figure 2), likely due to the involvement of carotenoids in photo-oxidative degradation, as suggested by previous reports (Cao et al., 2012).

Previously, an *SGR*-silenced tomato mutant (*gf*, *green flesh*) was reported to contain both plastoglobules (indicative chromoplast characteristics) and thylakoid structures (indicative chloroplast characteristics) in the cells of its ripe fruit (Cheung et al., 1993). In this study, we also examined the phenotypes of *SGR*-silenced *N. benthamiana* leaves. Using virus-induced gene silencing (VIGS), we significantly repressed the expression of *SGR* compared to the *GFP* mock control (VIGS-GFP) (Supplemental Figure S4A). However, the leaves from the *SGR*-silenced seedlings (VIGS-NbSGR) did not display distinct phenotypes compared to those from the VIGS-GFP control (Supplemental Figure S4, B and C). Additionally, we further overexpressed (*p*)*CrtB* to promote carotenoid biosynthesis in both VIGS lines. The

phenotypes of both lines were similar to those previously reported for the overexpression of (*p*)*CrtB* in wild-type *N. benthamiana*, where leaf regions exhibited an orange color and chromoplast-like structures were observed in their cells (Supplemental Figure S4, B and C) (Llorente et al., 2020).

SGR disassembles the photosynthetic complexes by initiating the overall degradation of chlorophylls in darkness

Continuous monitoring of the chlorophyll content of leaves overexpressing *SGR* in the dark for 5 days showed that the degradation of Chl *a* was observed initially, followed by the subsequent degradation of Chl *b* (Supplemental Figure S5A). This is consistent with the enzymatic activity characteristic of SGR, which exclusively accepts Chl *a* as its substrate (Shimoda et al., 2016). Simultaneously, the expression of *NYC1* and *PAO* was observed to have an approximately two-fold up-regulation, as well as a four-fold up-regulation of *PPH* (Supplemental Figure S5C), in line with the previous reports that SGR can activate Chl *b* degradation by inducing the expression of *NYC1*, so as to *PPH* and *PAO* to facilitate the complete degradation of chlorophylls by the "PAO/phyllobilin" pathway (Kuai et al., 2018; Sato et al., 2018; Ono et al., 2019).

To exam why darkness is more conducive to the enzyme activity of SGR, we measured the accumulation of Pheo *a*, the direct product of SGR, in *Arabidopsis pph* mutants transformed with a DEX-induced *SGR* expression system, which allowed Pheo *a* to accumulate upon SGR induction (Figure 3A). The results revealed a significantly higher accumulation of Pheo *a* in the dark compared with the treatment in the light, indicating Pheo *a* has enhanced stability under darkness (Figure 3, B and C). This property might facilitate the subsequent degradation of chlorophyll catabolic intermediates. Thereby, the accumulation of NCCs, the final products of the PAO/phyllobilin pathway initiated by SGR (Figure 1A), was measured in SGR-regions in either light or dark, and the results demonstrated a higher accumulation of NCCs in the dark than in the light, proving the appropriateness of darkness in this transient overexpression system (Supplemental Figure S6).

Chlorophylls are essential components of photosynthetic complexes. To assess whether the degradation of chlorophylls initiated by the overexpression of SGR in our

study also affected the structure of photosynthetic complexes, we preliminarily compared the abundance of D1, the chlorophyll-binding core component of the PSII reaction center, in the *EYFP*- and *SGR*-overexpressing leaves. Our immunoblot clearly revealed that D1 was not detectable in the *SGR*-overexpressing leaves (Supplemental Figure S5E). We then separated thylakoid membrane protein complexes by blue native (BN)-PAGE. While the protein complexes were partially disorganized by the overexpression of both *PPH* and *CLH1*, they were near-completely dismantled in the *SGR*-overexpressing samples (Figure 3D). Moreover, we performed immunoblotting analysis using an antibody against Lhcb2, the chlorophyll-binding protein of the light-harvesting complex LHCII. The *SGR*-overexpressing leaves were the only sample from which Lhcb2 could not be detected, in contrast to the *EYFP*-, *PPH*- and *CLH1*-overexpressing ones (Figure 3E). Therefore, it is possible that the degradation of chlorophyll initiated by SGR-catalyzed Mg dechelation destabilized the photosynthetic pigment-protein complexes.

Plastids in the orange regions have carotenoid-bearing structures resembling chromoplasts

In chloroplasts, chlorophylls but also carotenoids play an essential role in stabilizing the thylakoid membrane system. To investigate whether there were also structural changes in plastids in the dark-incubated SGR regions, we first performed optical microscopic observations. Needle-like orange crystals were frequently observed in plastids of the mesophyll cells from the orange regions, resembling those found in chromoplasts from the carotenoid-accumulating orange tissues of the cauliflower *or* mutant (Figure 4A) (Lu et al., 2006). As a control, those from the *EYFP*-overexpressing leaf region (EYFP-region) contained normal (green) chloroplasts (Figure 4A).

We further monitored the presence of chlorophylls and carotenoids in plastids of mesophyll cells by confocal microscopy, based on the differential autofluorescent properties of photosynthetic pigments (Egea et al., 2011; D'Andrea et al., 2014). Ripe tomato fruit pericarp, which contains predominantly chromoplasts, and mock-treated leaf, which contains mainly chloroplasts, were used as controls for comparisons. In ripe tomato pericarp cells, only the autofluorescence of carotenoids was detected. In contrast, mock-treated leaf cells only showed the autofluorescence of chlorophylls (Figure 4B).

In SGR-regions, however, plastids emitting only red autofluorescence (from chlorophylls), only green autofluorescence (from carotenoids), or an orange fluorescence due to green and red overlapping, were all observed (Figure 4B). Representative spectra from single plastids are depicted in Figure 4C. Plastids in the SGR region showed two peaks, corresponding to carotenoids and chlorophylls, respectively, indicating a transitional plastid type. Consistent with the fluorescence result, intact plastids isolated from the SGR-region using sucrose gradients also separated into two bands, a lighter orange fraction and a heavier green fraction (Figure 4D), in agreement with the reported lower density of chromoplasts compared to chloroplasts (Egea et al., 2011). The scenario of the SGR-region in which chloroplasts and the chromoplast-like plastids coexist resembles that of the breaker stage of ripening fruits in terms of pigment composition (Egea et al., 2010; D'Andrea et al., 2014).

To determine whether the orange plastids containing those crystal-like structures developed carotenoid-sequestering structures characteristic of chromoplasts, we carried out transmission electron microscopy (TEM) observations. The dark-incubated EYFP-regions exhibited chloroplasts with some electron-dense vesicles (plastoglobules) and well-organized photosynthetic thylakoid membranes and grana structures. The plastids of orange SGR-regions showed a proliferation of plastoglobules (a trend characteristic of chromoplasts) but retained the thylakoids and grana typical of chloroplasts, albeit with disintegrated structures (Figure 5). Most strikingly, these plastids showed undulating membranes that resembled the remnants of carotenoid crystal envelopes typical of crystalloid chromoplasts (Schweiggert and Carle, 2017). These undulating structures are usually formed during the preparation of the TEM sample, when the carotenoid crystals are lost, and the membranes covering them shrink and collapse.

Transcriptomic analysis indicated that SGR triggers chloroplast senescence

To illustrate the potential mechanism underlying this artificial plastid conversion in dark-incubated SGR-regions, we sequenced the transcriptomes of SGR- and EYFP-regions both in the light and in darkness. Principal component analysis of variance (PCA) was used to establish the degree of difference between different samples in an unbiased manner (Figure 6A). The close clustering of samples from the same group on the scatter plot indicates high sequencing quality and good biological reproducibility.

Light-exposed and dark-incubated SGR samples clustered together, rather than being clustered according to their different light-dependent phenotypes, suggesting that SGR played a primary role in shaping the observed patterns, while the light condition served as a secondary determinant. Between the transcriptomes of dark-treated SGR- (SGR/dark, SD) and EYFP- (EYFP/dark, ED) leaves (SD_vs_ED), there were a total of 12,743 differentially expressed genes (DEGs, p value<0.05; |fold change| >1), including 5,401 upregulated genes and 7,342 downregulated genes (Figure 6B). However, most of the DEGs from SD_vs_ED also show differential expression between the light-treated SGR- (SGR/light, SL) and EYFP- (EYFP/light, EL) regions (SL_vs_EL), or between the EYFP/dark and EYFP/light (ED_vs_EL). By excluding the DEGs shared with the two latter sample pairs, a total of 5,401 DEGs, including 2,254 upregulated genes and 3,147 downregulated genes, were identified as the gene repertoire that was specifically regulated by SGR and the dark treatment, that is, the gene clusters specifically associated with the orange phenotype (Figure 6C). These selected gene sets were subsequently utilized for comprehensive gene-ontology (GO) analysis.

Enrichment of GO terms in upregulated DEGs suggested a strong activation of protein degradation in SGR/dark samples, primarily facilitated by the vesicle-mediated transport (Supplemental Figure S7A), while GO terms enriched in downregulated DEGs indicated a repression of DNA replication and, further, of nuclear and cell division (Supplemental Figure S7B) (Gao et al., 2017; Pecenkova et al., 2017). Consistent with the GO enrichment analysis, a careful analysis of TEM images captured from SGR/dark samples showed clear corresponding endocytosis and chloroplast ‘blebbing’ in mesophyll cells, indicating degradation of plastid components and their transport to the vacuole by vesicles (Figure 6D) (Rodriguez-Furlan et al., 2019; Fisher et al., 2022). The electron density of the plastid stromal region in the SGR samples was also found to be lower than that of the EYFP controls, likely as a result of the loss of stromal materials (Figure 5) (Izumi et al., 2017).

Artificial differentiation of leaf chloroplasts into chromoplasts can be triggered by agroinfiltration of constructs expressing a bacterial phytoene synthase (CrtB), which results in a boost in carotenoid production without changes in the levels of chlorophylls (Llorente et al., 2020). While the previously reported GO term enrichment profile of

the CrtB-mediated artificial leaf chromoplastogenesis resembles that of ripening tomato fruit (Llorente et al., 2020), our profile exhibits more similarities with that of senescent *Arabidopsis* leaves (Supplemental Figure S8) (Woo et al., 2016), which is characterized by downregulation of photosynthesis-associated genes (*PAGs*) and an upregulation of senescence-associated genes (*SAGs*) (Biswal et al., 2012). The expression levels of representative *PAGs* and *SAGs*, including a senescence regulator *ORE1*, demonstrated a consistent outcome that SGR/dark samples showed a signal of senescence (Supplemental Figure S9) (Biswal et al., 2003; Balazadeh et al., 2010). Most strikingly, the number of plastids was observed to decrease, and the plastidial area exhibited enlargement in SGR/dark samples, also in agreement with a stressed and degraded plastid condition in a senescence scenario (Figure 6, E and F) (Krupinska, 2007; Fisher et al., 2022).

Because a small subset of plastidial proteins is encoded by the plastidial genome, similarly, we also compared the expression of those genes. However, our results showed that only a few genes, such as *PsaA* and *PsaB*, were down-regulated in the SGR/light (SL) group, reflecting a photodamage situation of these leaves, and the *rps* genes (*e.g.*, *rps11*/*14*/*15*) encoding the plastidial ribosomal proteins were down-regulated in dark-incubated samples, indicating a reduced chloroplast protein translation activity (Supplemental Figure S10).

SGR-induced plastid differentiation is independent of carotenoid biosynthesis

Chlorophylls and carotenoids are the two major classes of pigments in chloroplasts. In senescent leaves, both chlorophylls and carotenoids decrease as chloroplasts are transformed into gerontoplasts (Biswal et al., 2012), whereas in ripening fruits, the transformation from chloroplasts to chromoplasts is accompanied by the simultaneous down-regulation of chlorophyll biosynthesis and enhanced accumulation of carotenoids (Gapper et al., 2013). However, in our SGR-regions, the decrease in chlorophyll content by *SGR* overexpression did not dramatically alter the composition and contents of carotenoids (Supplemental Figure S5B). We actually detected a down-regulation, instead of the expected up-regulation, of genes involved in carotenoid biosynthesis (Supplemental Figure S5D). These results suggested that carotenoid synthesis was not enhanced by the overexpression of *SGR*.

To determine whether the *de novo* synthesis of carotenoids could contribute to the transformation from chloroplasts to the carotenoid-dominant plastids in the SGR-region, we treated *N. benthamiana* leaves overexpressing *SGR* or *EYFP* with norflurazon (NF) or 2-(4-chlorophenylthio)-triethylamine hydrochloride (CPTA) to block carotenoid synthesis at the level of phytoene desaturase or lycopene cyclase, respectively (Figure 7A) (Lu et al., 2019). Leaf bleaching associated with the activity of two inhibitors was clearly observed (Figure 7B) (Di et al., 2023). However, the treatments with either inhibitor did not change the characteristic orange color associated with *SGR*-overexpression (Figure 7A), and total carotenoid content remained largely unchanged (Figure 7C). This might indicate a relatively low turnover rate of carotenoids during the transition and confirms that carotenoid biosynthesis is not necessary for the formation of carotenoid-bearing structures in plastids from the SGR-region. Thereby, the plastid differentiation process observed here not only contrasts with the chromoplast differentiation in natural systems, such as during fruit ripening, but also differs from the artificial chloroplast-to-chromoplast differentiation in *N. benthamiana* leaves induced by the carotenoid biosynthetic enzyme CrtB, which involves induced production of carotenoids (but unchanged levels of chlorophylls) and it is completely aborted by the NF treatment (Llorente et al., 2020).

Discussion

Metabolic alterations are major drivers in the development of plastid ultrastructure

Both nuclear and plastid genes regulate plastid differentiation. A “molecular switch” was proposed to exist that can actively differentiate plastid types, such as the ORANGE (OR) chaperone protein, which was believed to specifically initiate chromoplastogenesis across different species (Lu et al., 2006; Lopez-Juez, 2007; Hermanns et al., 2020). However, more and more results are showing that metabolic perturbations are the main trigger for plastidial differentiation. For example, the role of OR in chromoplast differentiation can be mostly explained based on the capacity of this chaperone to promote the biosynthesis and sequestration of carotenoids (Welsch et al., 2018; Feder et al., 2019; Llorente et al., 2020; Zhou et al., 2023). Also, manipulation of phytoene levels by constitutively overexpressing phytoene synthase enzymes

promoted the differentiation of chloroplasts into chromoplast-like structures arising prematurely during fruit development in tomato (Fraser et al., 2007) or artificially developing in *N. benthamiana* leaves (Llorente et al., 2020). These reports all indicated that the promotion of carotenoid metabolism is able to initiate the transition of chloroplasts toward chromoplasts, which is marked by the appearance of the characteristic carotenoid-storing structures of chromoplasts such as lipid vesicles (plastoglobules) and crystalline bodies. Here, by overexpressing SGR, an enzyme that plays a common role in both ripening and senescence, we demonstrated that increased carotenoid production is not an absolute requirement for chromoplasts to develop. Instead, the degradation of chlorophylls can also initiate the formation of chromoplast-like structures from chloroplasts by an alternative route that does not require an induced production of carotenoids but the maintenance of their levels (e.g., by incubation in the dark, which prevents carotenoid photo-degradation).

Carotenoids deposited in SGR plastids might originate from photosynthetic complexes disassembled after SGR-mediated degradation of chlorophylls

In the chloroplast, carotenoids act as structural components and photoprotectors of the photosynthetic machinery, mostly in the form of chlorophyll-carotenoid-protein complexes (Vishnevetsky et al., 1999). For example, the ancillary carotenoids present in LHCs are required for their folding and stability and for broadening their energy absorption window, but LHC-associated carotenoids also protect the photosystems through a mechanism known as nonphotochemical quenching (NPQ), which safeguards against photodamage by regulating the energy flow and dissipating excess excitation energy as harmless heat (Sun et al., 2022). Thylakoid membranes are, therefore, the main site for the deposition and storage of synthesized carotenoids in chloroplasts (Li and Yuan, 2013). Given the results indicating that *de novo* synthesized carotenoids are not necessary for the orange leaf pigmentation (Figure 7), it is plausible to propose that the crystal-forming carotenoids in the plastid stroma originated from those involved in chloroplast structure, that is, those assembled within the photosynthetic complexes. The plastoglobules that proliferate in the chromoplast-like plastids present in orange sectors of SGR leaves might also contribute to storing the remaining carotenoids, protecting them from degradation (Morelli et al., 2022).

SGR-silenced mutants are type C stay-greens (also known as cosmetic stay-greens), which display inhibited chlorophyll degradation, but other aspects of senescence proceed normally (Thomas and Howarth, 2000), indicating that SGR specifically affects chlorophyll degradation. Meanwhile, SGR is associated with the first events of the destabilization of the LHC proteins, which are obligatory steps for the degradation of chlorophylls and antenna polypeptides (Dall'Osto et al., 2015), and there are numerous reports suggest that SGR is involved in dismantling CP complexes (Jiang et al., 2007; Park et al., 2007; Sato et al., 2007; Shimoda et al., 2016; Ying et al., 2021). SGR was proven to be able to extract Mg^{2+} not only from free chlorophyll but also from chlorophyll in the CP complexes (Shimoda et al., 2016). According to the previously suggested digestion sequence of the pigment-protein complexes, chlorophyll catabolic enzymes first degrade chlorophyll molecules bound to proteins, then chlorophyll-depleted apoproteins are immediately digested by some proteases. Here we propose that SGR disassembles the photosynthetic complexes by initiating the overall degradation of chlorophylls (Figure 3, D and E; Supplemental Figure S5, A, C and E), facilitating a rapid release of carotenoids composed in the complexes which aggregated in the plastid stroma later, ultimately leading to the formation of carotenoid crystals. Similar carotenoid composition and proportion between SGR-regions and EYFP controls, encompassing typical chloroplast-pigments like lutein, violaxanthin, neoxanthin, and β-carotene (Supplemental Figure S5B), provides additional corroboration supporting that carotenoids forming crystals in the plastid stroma were shed from the photosynthetic complexes (Schweiggert and Carle, 2017).

Darkness protects SGR-induced chlorophyll degradation by avoiding phototoxicity of chlorophyll catabolic intermediates

SGR is widely recognized as a key enzyme of chlorophyll breakdown upregulated during natural senescence and fruit ripening under normal growth light conditions (Ren et al., 2007; Sato et al., 2007; Barry et al., 2008), but our results (Supplemental Figure S3) along with previous studies (Jiang et al., 2011) both indicated that the overexpression of *SGR* resulted in leaf impairments when samples were exposed to light, while no detrimental phenotype was observed under dark conditions. Our data suggest that the dark environment in our system provided an optimal condition for the

degradation of SGR-induced chlorophylls and subsequent decomposition of photosynthetic complexes without causing phototoxicity (Figure 3, Supplemental Figures S1, S3 and S6). This promoted the release of carotenoids composed in the photosynthetic complexes and led to their later crystallization in the plastid stroma. Strikingly, the activity of SGR, which is also highly expressed in physiological processes like fruit ripening and senescence, was never observed to trigger photodamage, highlighting the significance of its detoxification mechanism under natural growth light conditions. The investigation of the mechanisms underlying SGR-induced light damage and the development of effective preventive strategies warrant further exploration.

SGR is the essential chlorophyll-breaking down enzyme involved in the transition of chloroplast

Chlorophylls are broken down through two different pathways. One starts from the dephytylation of chlorophylls by CLH1 or other dephytylase, which primarily facilitates chlorophyll salvage and recycling, and the other is the "PAO/phyllobilin" pathway initiated by the SGR-catalyzed Mg-dechelation (Figure 1A) (Kuai et al., 2018; Lin and Charng, 2021). From our results, the overexpression of *SGR*, *PPH* an *CLH1* all induced the degradation of chlorophylls, along with the accumulation of their breakdown products, and raised the carotenoid/chlorophyll ratio (Figure 2A, Supplemental Figure S1). However, only the *SGR*-overexpressing leaves showed the distinct bright orange phenotype, indicating that these two degradation pathways lead to different scenarios. This postulation was supported by our observation of the undetectable Lhcb2 protein and the destabilization of the photosynthetic protein complexes only in the *SGR*-overexpressing samples, suggesting that chlorophyll dephytylation is not associated with the transition from chloroplast to carotenoid-dominating plastids. PPH and PAO catalyze the hydrolysis of the phytol tail from pheophytin, and subsequent oxidation, respectively, beyond SGR (Figure 1A). Their overexpression could not copy the bright orange phenotype either (Figure 2), demonstrating a critical role of SGR in the degradation of chlorophylls and in the plastid transition. Moreover, in a recent study, although the overexpression of a bacterial phytoene synthase gene (*CrtB*) induced carotenoid biosynthesis and raised the

carotenoid/chlorophyll ratio in *N. benthamiana*, there was no similar plastid transition from chloroplast to chromoplast-like plastid as we observed in the *SGR*-overexpressing leaves (Llorente et al, 2020). Therefore, the formation of chromoplast-like plastids in our study is likely specific to Mg-dechelation catalyzed by *SGR* overexpression for chlorophyll degradation, instead of being a general consequence of chlorophyll breakdown by the other pathway and the raised carotenoid/chlorophyll ratio.

Tomato (*Solanum lycopersicum*) *green-flesh* (*gf*) and pepper (*Capsicum annuum*) *chlorophyll retainer* (*cl*) are SGR loss-of-function mutants by a single amino acid substitution (Barry et al., 2008). Significant levels of thylakoid stacks remained in ripe *gf* fruits while chromoplast development was not impaired, indicating chromoplast development was an independent process from chlorophyll breakdown and rendering the authors proposed that SGR was necessary for proper chloroplast deterioration in chloroplast-chromoplast transition (Cheung et al., 1993). Here, by overexpressing *SGR* under specific spatial-temporal conditions, we clearly demonstrated that *SGR*, the mutated locus of the *gf* and *cl* mutants, cues the onset of chloroplast deterioration, making the plastid convert into a transitional stage characterized by typical chromoplast structural features and a transcriptomic scenario associated with senescence, indicating the expression of *SGR* as an important signal to initiate chloroplast deterioration as the first developmental stage in chromoplastogenesis in ripening fruits and gerontoplast differentiation in senescing green leaves (Figure 8). Our results also showed that, in addition to active plastid differentiation processes regulated by developmental factors, the plastid has the ability to adapt its ultrastructure to real-time metabolic composition.

Taken together, our findings propose that the fate of a chloroplast is determined by a combination of developmental and environmental factors (*e.g.*, those triggering fruit ripening or leaf senescence) by pathways that involve SGR-catalyzed chlorophyll degradation and other processes, such as the production of huge amounts of carotenoids during fruit ripening (to form chromoplasts) or the remobilization of nutrients during senescence (to form gerontoplasts). Our results provide a new insight and interpretation of plastid differentiation. It can be postulated that the morphology of plastids is shaped by a series of different independent metabolic events, with each event giving rise to a specific plastid structure. We, therefore, highlight the adaptive capacity of plastid

ultrastructure in response to variations in metabolic constituents, providing a perspective that contributes to the elucidation of novel plastid types across diverse environments (Sierra et al., 2023). As a corollary of our work, it can be concluded that the classification of non-photosynthetic plastids as chromoplasts, gerontoplasts, *etc*., should be reconsidered as the arising picture indicates that plastids are extremely dynamic organelles with transition stages aimed to adapt their ultrastructure to their changing metabolic composition.

Materials and Methods

Plant materials and growth conditions

N. benthamiana and *Arabidopsis thaliana pOpON:SGR1-FLAG/pph* in Columbia-0 background (kindly provided by Dr. Ryouichi Tanaka, Hokkaido University, Japan) were grown under standard conditions as described previously (Shimoda et al., 2016; Majer et al., 2017; Sun et al., 2019). For dark incubation, *N. benthamiana* leaves after agroinfiltration were kept attached to the plant or detached on top of water-soaked filter paper in Petri dishes covered with aluminum foil; *A. thaliana* seedlings grown in pots were covered with aluminum foil after DEX induction. Collected plant material was frozen in liquid nitrogen, lyophilized, homogenized to a fine powder, and stored at –80°C till further analyses.

Gene constructs

Full-length open reading frames (ORFs) of *NbSGR* (*Niben101Scf00490g01040.1*), *CaSGR1* (*Capana01g000359*), *AtPPH* (*At5g13800*), *AtPAO* (*At3g44880*), *AtCLH1* (*At1g19670*), *AtCLD1* (*At5g38520*), *AtNYC1* (*At4g13250*) and *AtNOL* (*At5g04900*) were PCR amplified using the primer pairs listed in Supplemental Table S1, and (*p*)*CrtB* was cloned as described previously (Llorente et al., 2020). All amplicons were subsequently cloned into the *Nco* I site of pCNHP by the in-fusion technology (Kong et al., 2020). EYFP was used as a negative control.

Transient expression assays

Each construct was introduced into *Agrobacterium tumefaciens* strain GV3101, and a single transformed colony was picked and inoculated overnight in 10 mL Luria-Bertani medium supplemented with rifampicin (50 μg mL^{-1}), gentamycin (50 μg mL^{-1}), and kanamycin (50 mL^{-1}) at 200 rpm and 28°C. Bacterial cells were collected by centrifugation and then resuspended in the agroinfiltration buffer (10 mM $MgCl_2$, 10 mM MES, 200 μM acetosyringone, pH 5.6) to achieve OD_{600} = 0.5. The mixture was further incubated at 28°C and 200 rpm for 1.5 h before infiltration. For pharmacological treatments, NF (40 μM) or CPTA (50 μM) was added into the mixture immediately before infiltration. The second or third youngest leaves of 4- to 6-week-old *N. benthamiana* plants were infiltrated with either a single *A. tumefaciens* culture or a mixture of equal amounts of different cultures following the procedure described previously (Sparkes et al., 2006).

VIGS of *NbSGR*

To silence the expression of *NbSGR* in *N. benthamiana*, we used the VIGS strategy as described previously (Wang et al., 2018). A 300-bp fragment of *NbSGR* with very low sequence similarities with other genes was cloned into pTRV2. As the negative control, a pTRV2-GFP vector that targets an absent *GFP* sequence was used. Gene expression analysis was conducted as described previously (Wang et al., 2018). Transcript abundance of *NbEF-1α* was used as an internal control (Ahmed et al., 2020). Primers used here are listed in Supplemental Table S1.

Metabolite analysis

Pigments were purified from 4 mg lyophilized leaf tissue, and profiled by HPLC using an Agilent 1260 system (Agilent, Santa Clara, CA, USA) with a reverse-phase Spherisorb ODS2 column (5 μm, 4.6 × 250 mm, Waters, Milford, MA, USA) as described previously (Huang et al., 2017; Wang et al., 2019). Canthaxanthin was used as an internal standard. NCCs were extracted from fresh leaf tissue, analyzed by HPLC, and named according to the nomenclature for chlorophyll catabolites as described previously (Ginsburg and Matile, 1993; Pružinská et al., 2003). The spectrum of each constituent was compared with published authentic data to further confirm the peak

identity (Hörtensteiner, 1999). At least three replicates were performed for each sample.

Trypan blue staining

Trypan blue was dissolved in lactophenol solution (phenol/lactic acid/glycerol/water, 1:1:1:1, v/v/v/v) at 0.01% (w/v). Leaves were immersed in staining solution for 20 min, and then destained in 95% (v/v) ethanol. Images were captured under a stereomicroscope.

Protein extraction, western blot and blue-native (BN)-PAGE analysis

Total proteins were extracted by homogenization of 300 mg fresh leaf tissue in 1 mL lysis buffer containing 50 mM Tris-HCl, pH 7.5, 150 mM NaCl, 5% (v/v) glycerol, 0.05% (v/v) Nonidet P-40, 1 mM $MgCl_2$, 10 mM DTT, 1 mM phenylmethylsulfonyl fluoride, and 1 × Protease Inhibitor Cocktail (NEB). The mixture was incubated in a rotatory device at 4°C for 15 min, then centrifuged at 4°C, 3,000 g for 15 min. The supernatant was further centrifuged at 4°C, 16,000 g for 30 min, and the protein concentration was measured using the BCA assay (Smith et al., 1985).

Protein samples were mixed with 5 × SDS loading buffer (Green and Sambrook, 2012), heated at 95°C for 10 min, separated on 15% SDS-polyacrylamide gel and subsequently blotted onto polyvinylidene difluoride (PVDF) membrane (Millipore) for immunodetection. The antibodies against Lhcb2 and PsaA/D1 were purchased from Agrisera (Vännäs, Sweden), and antibody against ACTIN was purchased from Sangon (Shanghai, China). Horseradish peroxidase (HRP)-conjugated secondary antibody against rabbit IgG was from Sangon (Shanghai, China). Common protocols and the manufacturers' manuals for SDS-PAGE, blotting, and immunodetection using the BeyoECL Star Western Blotting Substrate (Beyotime) were followed (Green and Sambrook, 2012). BN-PAGE was performed using 4–14% acrylamide gradient gels according to the method described before (Zhou et al., 2017). For each lane, 60 μg protein was loaded.

Microscopy

Leaf materials used for optical and confocal microscopy were torn carefully by a pair of tweezers from interested leaf sectors and placed between a glass slide and a coverslip. Detection of chlorophylls and carotenoids by confocal laser scanning microscope was performed as previously described (Egea et al., 2011; D'Andrea et al., 2014). Fluorescence emission spectra were acquired with excitation at 488 nm. The emitted fluorescence between 649–693 nm was collected for chlorophylls, and that between 493–589 nm was for carotenoids. Emission spectra were recorded between 500–700 nm. Transmission electron microscopy of plant leaves was performed as previously described (D'Andrea et al., 2018).

Plastid isolation

Plastids of leaf tissue were isolated with a discontinuous sucrose gradient essentially as described previously with some modifications (Wang et al., 2013). Briefly, 2 g fresh leaf tissue was homogenized in 30 mL ice-cold extraction buffer (300 mM sorbitol, 50 mM Tris-HCl, pH 8.0, 5 mM EDTA, pH 8.0, and 0.1% β-mercaptoethanol) and filtered through four layers of miracloth. The filtrate was centrifuged at 700 g for 10 min at 4°C. The supernatant was further centrifuged at 2,000 g for 10 min at 4°C. The crude plastid pellet was gently suspended in 1 mL extraction buffer, overlaid on a 52% sucrose (w/v, in 50 mM Tris-HCl, 25 mM EDTA, pH 8.8) and 30% sucrose (w/v, in 50 mM Tris-HCl, 25 mM EDTA, pH 8.0) discontinuous gradient, and centrifuged at 50,000 g for 30 min at 4°C.

DEX treatment

A. thaliana seedlings grown on soil for 2 weeks were used for DEX induction. DEX stock was prepared as 20 mM in dimethyl sulfoxide (DMSO). Plants were sprayed with a DEX solution (10 μM diluted in water) supplemented with 0.015% Silwet L-77, then incubated under growth light or darkness for 48 h.

Statistical analyses

For each sample, 3 replicates were used for RNAseq analysis by Novogene (Beijing,

China). Principal component analysis (PCA) was performed using the prcomp function in R. Differentially expressed genes (DEGs) were identified with the DESeq2 statistical method (Love et al., 2014). The resulting gene list was filtered using cut-offs of adjusted *p* value < 0.05 and $\log_2$-transformed fold change ($\log_2$FC) > 1 for upregulated genes and < 1 for down-regulated genes. GO enrichment analysis and the comparison between different samples were performed as previously described (Llorente et al., 2020). Variation analyses were performed using GraphPad Prism 8.0 (GraphPad Software). Heatmaps were made using the pheatmap package in R (https://cran.r-project.org/web/packages/pheatmap/index.html).

Acknowledgements and Funding

The authors are grateful to Jose Perez-Beser and the staff at the IBMCP Metabolomics Platform, and Zihan Ge from Nanjing University, for technical support, to Dr. Ryouichi Tanaka (Hokkaido University, Japan) for providing the *pOpON:SGR1-FLAG*/*pph* mutant, and to Dr. Li Li (Cornell University, USA) for the constructive discussions during the research.

This work was funded by grants from the Seed Industry Revitalization Project of Jiangsu Province of China (No. JBGS[2021]033) and the National Natural Science Foundation of China (No. 32470271) to S.L., and from Spanish MCIN/AEI/10.13039/501100011033 and European NextGeneration EU/PRTR and PRIMA programs to M.R.-C. (PID2023-149584NB-I00, PID2020-115810GB-I00, and UToPIQ-PCI2021-121941). M.R.-C. is also supported by Generalitat Valenciana (PROMETEU/2021/056 and AGROALNEXT/2022/067) and the MCIN/AEI-funded Spanish Carotenoid Network, CaRed (RED2022-134577-T). H.Z.'s visiting stay at IBMCP-Universitat Politècnica de València was sponsored by the China Scholarship Council (CSC).

Author contributions

H.Z., M.R.-C., and S.L. designed research, analyzed data, and wrote the paper; H.Z., S.T.-M., and X.H. performed research.

Declare of interests: Authors declare that they have no competing interests.

Supplementary data

Figure S1. Chlorophyll degradation products in leaves overexpressing different chlorophyll catabolic genes in dark and light.

Figure S2. The overexpression of other chlorophyll-degrading enzymes cannot produce the orange leaf phenotype in either light or dark.

Figure S3. *SGR*-overexpression leaf regions are susceptible to photodamages.

Figure S4. Phenotypes of (*p*)*CrtB*-overexpressing leaf regions in *SGR*-silenced *N. benthamiana* plants.

Figure S5. Pigment contents, corresponding gene expression and photosynthetic protein complex analysis.

Figure S6. NCCs accumulate mainly in dark-incubated SGR samples.

Figure S7. Representative enriched GO terms of the differential expressed genes.

Figure S8. Transcriptome of the dark-incubated *SGR*-overexpressing leaves resembles that of senescent leaves.

Figure S9. The expression of photosynthesis- and senescence-associated genes in dark-incubated *SGR* samples.

Figure S10. The expression of plastid-encoded genes in different *SGR* samples.

Table S1. Primers used in this work**.**

Supplemental Data Set S1. Accession numbers for *N. benthamiana* genes involved in chlorophyll degradation and carotenoid biosynthesis.

Supplemental Data Set S2. GO analysis of DEGs.

Supplemental Data Set S3. Accession numbers of photosynthesis- and senescence-associated *N. benthamiana* genes in dark-incubated *SGR* samples.

References

Ahmed RI, Ren A, Yang D, Ding A, Kong Y (2020). Identification and characterization of pectin related gene *NbGAE6* through virus-induced gene silencing in *Nicotiana benthamiana*. Gene **741:** 144522

Balazadeh S, Wu A, Mueller-Roeber B (2010) Salt-triggered expression of the ANAC092-dependent senescence regulon in *Arabidopsis thaliana*. Plant Signal Behav **5:** 733–735

Barry CS, McQuinn RP, Chung M-Y, Besuden A, Giovannoni JJ (2008) Amino acid substitutions in homologs of the STAY-GREEN protein are responsible for the *green-flesh* and *chlorophyll retainer* mutations of tomato and pepper. Plant Physiol **147:** 179–187

Biswal B, Mohapatra PK, Biswal UC, Raval MK (2012) Leaf senescence and transformation of chloroplasts to gerontoplasts. *In* JJ Eaton-Rye, BC Tripathy, TD Sharkey, eds, Photosynthesis: Plastid Biology, Energy Conversion and Carbon Assimilation. Springer, New York, pp. 217–230

Biswal UC, Biswal B, Raval MK (2003) Transformation of chloroplast to gerontoplast. *In* Chloroplast biogenesis. Springer, New York, pp. 155–242

Cao H, Zhang J, Xu J, Ye J, Yun Z, Xu Q, Xu J, Deng X (2012) Comprehending crystalline β-carotene accumulation by comparing engineered cell models and the natural carotenoid-rich system of citrus. J Exp Bot **63:** 4403–4417

Cheung AY, McNellis T, Piekos B (1993) Maintenance of chloroplast components during chromoplast differentiation in the tomato mutant *Green Flesh*. Plant Physiol **101:** 1223–1229

D'Andrea L, Amenós M, Rodriguez-Concepción M (2014) Confocal laser scanning microscopy detection of chlorophylls and carotenoids in chloroplasts and chromoplasts of tomato fruit. *In* M Rodríguez-Concepción ed, Plant Isoprenoids: Methods and Protocols. Springer, New York, pp. 227–232

Dall'Osto L, Bressan M, Bassi R (2015) Biogenesis of light harvesting proteins. Biochim Biophys Acta **1847:** 861–871

Di XN, Ortega-Alarcon D, Kakumanu R, Iglesias-Fernandez J, Diaz L, Baidoo EEK, Velazquez-Campoy A, Rodríguez-Concepción M, Perez-Gil J (2023) MEP pathway products allosterically promote monomerization of deoxy-D-xylulose-5-phosphate synthase to feedback-regulate their supply. Plant Commun **4:** 100512

Egea I, Barsan C, Bian W, Purgatto E, Latché A, Chervin C, Bouzayen M, Pech J-C (2010) Chromoplast differentiation: current status and perspectives. Plant Cell Physiol **51:** 1601–1611

Egea I, Bian W, Barsan C, Jauneau A, Pech J-C, Latché A, Li Z, Chervin C (2011) Chloroplast to chromoplast transition in tomato fruit: spectral confocal microscopy analyses of carotenoids and chlorophylls in isolated plastids and time-lapse recording on intact live tissue. Ann Bot **108:** 291–297

Feder A, Chayut N, Gur A, Freiman Z, Tzuri G, Meir A, Saar U, Ohali S, Baumkoler F, Gal-On A, Shnaider Y, Wolf D, Katzir N, Schaffer A, Burger J, Li L, Tadmor Y (2019) The role of carotenogenic metabolic flux in carotenoid accumulation and chromoplast differentiation: lessons from the melon fruit. Front Plant Sci **10:** 1250

Fisher KE, Krishnamoorthy P, Joens MS, Chory J, Fitzpatrick JAJ, Woodson JD (2022) Singlet oxygen leads to structural changes to chloroplasts during their

degradation in the *Arabidopsis thaliana plastid ferrochelatase two* mutant. Plant Cell Physiol **63:** 248–264

Fraser PD, Enfissi EM, Halket JM, Truesdale MR, Yu D, Gerrish C, Bramley PM (2007) Manipulation of phytoene levels in tomato fruit: effects on isoprenoids, plastids, and intermediary metabolism. Plant Cell **19:** 3194–3211

Gao C, Zhuang X, Shen J, Jiang L (2017) Plant ESCRT complexes: moving beyond endosomal sorting. Trends Plant Sci **22:** 986–998

Gapper NE, McQuinn RP, Giovannoni JJ (2013) Molecular and genetic regulation of fruit ripening. Plant Mol Biol **82:** 575–591

Green MR, Sambrook J (2012) *Molecular Cloning: A Laboratory Manuel.* Cold Spring Harbor Laboratory Press, Cold Springer Harbor, NY

Gruszecki WI (2013) Structure–function relationship of the plant photosynthetic pigment–protein complex LHCII studied with molecular spectroscopy techniques. Adv Protein Chem Struct Biol **93:** 81–93

Hermanns AS, Zhou X, Xu Q, Tadmor Y, Li L (2020) Carotenoid pigment accumulation in horticultural plants. Hortic Plant J **6:** 343–360

Horie Y, Ito H, Kusaba M, Tanaka R, Tanaka A (2009) Participation of chlorophyll *b* reductase in the initial step of the degradation of light-harvesting chlorophyll *a*/*b*-protein complexes in *Arabidopsis*. J Biol Chem **284:** 17449–17456

Hörtensteiner S (2006) Chlorophyll degradation during senescence. Annu Rev Plant Biol **57:** 55–77

Izumi M, Ishida H, Nakamura S, Hidema J (2017) Entire photodamaged chloroplasts are transported to the central vacuole by autophagy. Plant Cell **29:** 377–394

Jiang H, Chen Y, Li M, Xu X, Wu G (2011) Overexpression of *SGR* results in oxidative stress and lesion-mimic cell death in rice seedlings. J Integr Plant Biol **53:** 375–387

Jiang H, Li M, Liang N, Yan H, Wei Y, Xu X, Liu J, Xu Z, Chen F, Wu G (2007) Molecular cloning and function analysis of the *stay green* gene in rice. Plant J **52:** 197–209

Krupinska K (2007) Fate and activities of plastids during leaf senescence. *In* RR Wise, JK Hoober, eds, The Structure and Function of Plastids. Springer, New York, pp 433–449

Kuai B, Chen J, Hörtensteiner S (2018) The biochemistry and molecular biology of chlorophyll breakdown. J Exp Bot **69:** 751–767

Lancien M, Lea PJ, Azevedo RA (2007) Amino acid synthesis in plastids. *In* RR Wise, JK Hoober, eds, The Structure and Function of Plastids. Springer, New York, pp 355–385

Li L, Yuan H (2013) Chromoplast biogenesis and carotenoid accumulation. Arch Biochem Biophys **539:** 102–109

Lin Y-P, Charng Y-y (2021) Chlorophyll dephytylation in chlorophyll metabolism: a simple reaction catalyzed by various enzymes. Plant Sci **302:** 110682

Liu Y, Ye J, Zhu M, Atkinson RG, Zhang Y, Zheng X, Lu J, Cao Z, Peng J, Shi C, Xie Z, Larkin RM, Nieuwenhuizen NJ, Ampomah-Dwamena C, Chen C, Wang R, Luo X, Cheng Y, Deng X, Zeng Y (2024) Multi-omics analyses reveal the importance of chromoplast plastoglobules in carotenoid accumulation in citrus fruit. Plant J **117:** 924–943

Ljubešić N, Wrischer M, Devidé Z (1991) Chromoplasts – the last stages in plastid development. Int J Dev Biol **35:** 251–258

Llorente B, Torres-Montilla S, Morelli L, Florez-Sarasa I, Matus JT, Ezquerro M, D'Andrea L, Houhou F, Majer E, Picó B, Cebolla J, Troncoso A, Fernie AR, Daròs JA, Rodriguez-Concepcion M (2020) Synthetic conversion of leaf chloroplasts into carotenoid-rich plastids reveals mechanistic basis of natural chromoplast development. Proc Natl Acad Sci USA **117:** 21796–21803

López-Juez E (2007) Plastid biogenesis, between light and shadows. J Exp Bot **58:** 11–26

Lu P, Wang S, Grierson D, Xu C (2019) Transcriptomic changes triggered by carotenoid biosynthesis inhibitors and role of *Citrus sinensis phosphate transporter 4;2* (*CsPHT4;2*) in enhancing carotenoid accumulation. Planta **249:** 257–270

Lu S, Eck JV, Zhou X, Lopez AB, O'Halloran DM, Cosman KM, Conlin BJ, Paolillo DJ, Garvin DF, Vrebalov J, Kochian LV, Küpper H, Earle ED, Cao J, Li L (2006) The cauliflower *Or* gene encodes a DnaJ cysteine-rich domain-containing protein that mediates high levels of β-carotene accumulation. Plant Cell **18:** 3594–3605

Luo Z, Zhang J, Li J, Yang C, Wang T, Ouyang B, Li H, Giovannoni J, Ye Z (2013) A STAY-GREEN protein SlSGR1 regulates lycopene and β-carotene accumulation by interacting directly with SlPSY1 during ripening processes in tomato. New Phytol **198:** 442–452

Morelli L, Torres-Montilla S, Glauser G, Shanmugabalaji V, Kessler F, Rodriguez-Concepcion M (2022) Novel insights into the contribution of plastoglobules and reactive oxygen species to chromoplast differentiation. New Phytol **237:** 1696–1710

Nisar N, Li L, Lu S, Khin NC, Pogson BJ (2015) Carotenoid metabolism in plants. Mol Plant **8:** 68–82

Ono K, Kimura M, Matsuura H, Tanaka A, Ito H (2019) Jasmonate production through chlorophyll *a* degradation by Stay-Green in *Arabidopsis thaliana*. J Plant Physiol **238:** 53–62

Park S-Y, Yu J-W, Park J-S, Li J, Yoo S-C, Lee N-Y, Lee S-K, Jeong S-W, Seo HS, Koh H-J, Jeon J-S, Park Y-I, Paek N-C (2007) The senescence-induced staygreen protein regulates chlorophyll degradation. Plant Cell **19:** 1649–1664

Pečenková T, Marković V, Sabol P, Kulich I, Žárský V (2017) Exocyst and autophagy-related membrane trafficking in plants. J Exp Bot **69:** 47–57

Pfannschmidt T (2010) Plastidial retrograde signalling – a true "plastid factor" or just metabolite signatures? Trends Plant Sci **15:** 427–435

Ren G, An K, Liao Y, Zhou X, Cao Y, Zhao H, Ge X, Kuai B (2007) Identification of a novel chloroplast protein AtNYE1 regulating chlorophyll degradation during leaf senescence in Arabidopsis. Plant Physiol **144:** 1429–1441

Roca M, Hornero-Méndez D, Gandul-Rojas B, Mínguez-Mosquera MI (2006) Stay-green phenotype slows the carotenogenic process in *Capsicum annuum* (L.) fruits. J Agric Food Chem **54:** 8782–8787

Rodriguez-Furlan C, Domozych D, Qian W, Enquist P-A, Li X, Zhang C, Schenk R, Winbigler HS, Jackson W, Raikhel NV, Hicks GR (2019) Interaction between VPS35 and RABG3f is necessary as a checkpoint to control fusion of late compartments with the vacuole. Proc Natl Acad Sci USA **116:** 21291–

21301

Rolland N, Curien G, Finazzi G, Kuntz M, Maréchal E, Matringe M, Ravanel S, Seigneurin-Berny D (2012) The biosynthetic capacities of the plastids and integration between cytoplasmic and chloroplast processes. Annu Rev Genet **46:** 233–264

Sadali NM, Sowden RG, Ling Q, Jarvis RP (2019) Differentiation of chromoplasts and other plastids in plants. Plant Cell Rep **38:** 803–818

Sakuraba Y, Schelbert S, Park S-Y, Han S-H, Lee B-D, Andrès CB, Kessler F, Hörtensteiner S, Paek N-C (2012) STAY-GREEN and chlorophyll catabolic enzymes interact at light-harvesting complex II for chlorophyll detoxification during leaf senescence in *Arabidopsis*. Plant Cell **24:** 507–518

Sato T, Shimoda Y, Matsuda K, Tanaka A, Ito H (2018) Mg-dechelation of chlorophyll *a* by Stay-Green activates chlorophyll *b* degradation through expressing Non-Yellow Coloring 1 in *Arabidopsis thaliana*. J Plant Physiol **222:** 94–102

Sato Y, Morita R, Nishimura M, Yamaguchi H, Kusaba M (2007) Mendel's green cotyledon gene encodes a positive regulator of the chlorophyll-degrading pathway. Proc Natl Acad Sci USA **104:** 14169–14174

Schweiggert RM, Carle R (2017) Carotenoid deposition in plant and animal foods and its impact on bioavailability. Crit Rev Food Sci Nutr **57:** 1807–1830

Shimoda Y, Ito H, Tanaka A (2016) Arabidopsis *STAY-GREEN*, Mendel's green cotyledon gene, encodes magnesium-dechelatase. Plant Cell **28:** 2147–2160

Sierra J, Escobar-Tovar L, Leon P (2023) Plastids: diving into their diversity, their functions, and their role in plant development. J Exp Bot **74:** 2508–2526

Smith PK, Krohn RI, Hermanson GT, Mallia AK, Gartner FH, Provenzano MD, Fujimoto EK, Goeke NM, Olson BJ, Klenk DC (1985) Measurement of protein using bicinchoninic acid. Anal Biochem **150:** 76–85

Solymosi K, Lethin J, Aronsson H (2018) Diversity and plasticity of plastids in land plants. *In* E. Maréchal ed, Plastids: Methods and Protocols. Springer, New York, pp. 55–72

Sun T, Rao SM, Zhou X, Li L (2022) Plant carotenoids: recent advances and future perspectives. Mol Hortic **2:** 43897

Thomas H, Howarth CJ (2000) Five ways to stay green. J Exp Bot **51:** 329–337

Vishnevetsky M, Ovadis M, Vainstein A (1999) Carotenoid sequestration in plants: the role of carotenoid-associated proteins. Trends Plant Sci **4:** 232–235

Wang Q, Huang X-Q, Cao T-J, Zhuang Z, Wang R, Lu S. (2018). Heteromeric geranylgeranyl diphosphate synthase contributes to carotenoid biosynthesis in ripening fruits of red pepper (*Capsicum annuum* var. *conoides*). J Agric Food Chem **66:** 11691–11700

Wang Y-G, Zhang Y-M, Wang Y-H, Zhang K, Ma J, Hang J-X, Su Y-T, Tan S-S, Liu H, Xiong A-S, Xu Z-S (2024) The *Y* locus encodes a REPRESSOR OF PHOTOSYNTHETIC GENES protein that represses carotenoid biosynthesis via interaction with APRR2 in carrot. Plant Cell **36:** 2798–2817

Welsch R, Zhou X, Yuan H, Álvarez D, Sun T, Schlossarek D, Yang Y, Shen G, Zhang H, Rodriguez-Concepcion M, Thannhauser TW, Li L (2018) Clp protease and OR directly control the proteostasis of phytoene synthase, the crucial enzyme for carotenoid biosynthesis in *Arabidopsis*. Mol Plant **11:** 149–

162

Wen X, Heller A, Wang K, Han Q, Ni Y, Carle R, Schweiggert R (2020) Carotenogenesis and chromoplast development during ripening of yellow, orange and red colored *Physalis* fruit. Planta **251:** 95

Woo HR, Koo HJ, Kim J, Jeong H, Yang JO, Lee IH, Jun JH, Choi SH, Park SJ, Kang B, Kim YW, Phee B-K, Kim JH, Seo C, Park C, Kim SC, Park S, Lee B, Lee S, Hwang D, Nam HG, Lim PO (2016) Programming of plant leaf senescence with temporal and inter-organellar coordination of transcriptome in Arabidopsis. Plant Physiol **171:** 452–467

Yang YN, Safarova RB, Park S-Y, Sakuraba Y, Oh M-H, Zulfugarov IS, Lee CB, Tanaka A, Paek N-C, Lee C-H (2019) Chlorophyll degradation and light-harvesting complex II aggregate formation during dark-induced leaf senescence in Arabidopsis pheophytinase mutants. J Plant Biol **62:** 27–38

Ying C, Wataru Y, Ayumi T, Tanaka R, Hisashi I (2021) Degradation of the photosystem II core complex is independent of chlorophyll degradation mediated by Stay-Green Mg^{2+} dechelatase in *Arabidopsis*. Plant Sci **307:** 110902

Zhou F, Wang CY, Gutensohn M, Jiang L, Zhang P, Zhang D, Dudareva N, Lu S (2017) A recruiting protein of geranylgeranyl diphosphate synthase controls metabolic flux toward chlorophyll biosynthesis in rice. Proc Natl Acad Sci USA **114:** 6866–6871

Zhou X, Sun T, Owens L, Yang Y, Fish T, Wrightstone E, Lui A, Yuan H, Chayut N, Burger J, Tadmor Y, Thannhauser T, Guo W, Cheng L, Li L (2023) Carotenoid sequestration protein FIBRILLIN participates in CmOR-regulated β-carotene accumulation in melon. Plant Physiol **193:** 643–660

Figure Legends

Figure 1. Transient overexpression of *SGR* in dark-incubated leaves transforms the color from green to bright orange.

(A) Chlorophyll breakdown pathway. Abbreviations for enzymes are: NYC1, Non-Yellow Coloring 1; NOL, NYC1-like; HCAR, hydroxymethyl chlorophyll *a* reductase; CLH, chlorophyllase; CLD1, chlorophyll dephytylase1; SGR, Stay-Green; PPH, pheophytinase; PAO, pheophorbide *a* oxygenase; and RCCR, red chlorophyll catabolite reductase. Abbreviations for metabolites are: Chl *b*, chlorophyll *b*; Chl *a*, chlorophyll *a*; Pheo *a*, pheophytin *a*; Pheide *a*, pheophorbide *a*; pFCC, primary fluorescent chlorophyll catabolite; and NCCs, nonfluorescent chlorophyll catabolites. **(B)** Representative image of dark-incubated *N. benthamiana* leaf overexpressed *SGR* and *EYFP*.

Figure 2. The overexpression of *SGR* leads to the most conspicuous alteration in the carotenoid-chlorophyll ratio.

Representative images of leaves overexpressing different chlorophyll catabolic enzymes in the dark **(A)** and in the light **(B)**. Levels of chlorophylls (Chl) and carotenoids (Car), and the carotenoid-to-chlorophyll ratio (Ca-/Chl) in leaves overexpressing different genes are provided below the images. Each of the chlorophyll catabolic enzymes was overexpressed by infiltration in the left part of a leaf, with *EYFP* in the right part as a control. The pigment level is expressed as the ratio of its corresponding peak area to the internal standard peak area (canthaxanthin) calculated from the HPLC profile. Data are means ± SE (n = 8). Asterisks indicate significant differences between the enzymes and the *EYFP* control (t-test, **, $P < 0.01$ ****, $P < 0.0001$ or better). Chl *a*, chlorophyll *a*; Chl *b*, chlorophyll *b*; β-car, β-carotene; Lut, lutein; Vio, violaxanthin; Neo, neoxanthin.

Figure 3. SGR disassembles the photosynthetic complexes by initiating the overall degradation of chlorophylls in darkness.

(A) Scheme showing the accumulation of pheophytin *a* (Pheo *a*) by the dexamethasone (DEX)-induced expression of *SGR1* for 48h in 2-week-old *Arabidopsis thaliana*

pOpON:SGR1-FLAG/pph plants. Pheide *a*, pheophorbide *a*. **(B)** HPLC analysis of the accumulation of Pheo *a* in *Arabidopsis* plants treated by DEX in the light (DEX-dark) and the dark (DEX-dark). Absorption spectrum of Pheo *a* was shown as an inset. **(C)** Quantification of Pheo *a* accumulation in **(B)**. The level is expressed as the [Pheo *a* peak area/internal standard peak area] ratio calculated from the HPLC profile. Data are means ± SE ($n = 3$). Asterisks indicate significant differences between the plants treated in the dark and in the light (*t* test, *, $P < 0.05$). **(D)** Thylakoid membrane protein complexes separated by BN-PAGE. An equal amount of proteins (60 μg) from indicated overexpression leaves was loaded in each lane. **(E)** Immunoblot analysis of Lhcb2 protein in each of the indicated overexpression leaves.

Figure 4. Plastids in orange SGR-region show carotenoid-bearing structures.

(A) Microscopic observation of mesophyll cell plastids of *Nicotiana benthamiana* leaves overexpressing *SGR* and *EYFP*. Bar = 20 μm. **(B)** Confocal images of chlorophylls and carotenoids autofluorescence. Fresh pericarp tissue of ripe tomato fruit, *SGR*-overexpressing leaf region and mock-treated leaf region were observed. With an excitation wavelength at 488 nm, chlorophylls and carotenoids emitted fluorescence at 649–693 nm (red) and 493–589 nm (green), respectively. Therefore, structures containing mainly chlorophylls or carotenoids appear red or green, respectively, and those containing both pigments look orange. Bar = 20 μm. **(C)** Fluorescence emission spectra of ripe tomato pericarp tissue, *SGR*-overexpressed and mock-treated leaf regions under an excitation at 488 nm. Representative spectra were obtained from single plastids. The fluorescence emission range used to detect carotenoids (Car) and chlorophylls (Chl) is marked. **(D)** Separation of plastids isolated from SGR- and EYFP-regions on a sucrose gradient by centrifugation. Carotenoid-bearing plastids from the SGR-region showed an orange bank between the 52% and 30% sucrose layers.

Figure 5. Electron micrographs of mesophyll cell plastids of dark-incubated *N. benthamiana* leaves overexpressing *SGR* and *EYFP*.

Stacking granal thylakoids were observed in the control samples overexpressing *EYFP*, showing the chloroplast nature. Both plastoglobuli and undulating membrane structures for carotenoid storage were observed in the *SGR*-overexpressing samples. Bar = 1μm.

Figure 6. Transcriptomic analysis of *SGR*-induced gene expression.

(A) Principal component analysis (PCA) showing the first two components of variance among each biological replica of each sample. SD, *SGR*-overexpressing leaves collected after dark incubation; SL, *SGR*-overexpressing leaves collected after light incubation; ED, *EYFP*-overexpressing leaves collected after dark incubation; and EL, *EYFP*-overexpressing leaves collected after light incubation. **(B)** Number of differentially expressed genes (DEGs) between different pairs of samples. **(C)** Venn diagrams of overlapping DEGs from the three sets of samples compared in **(B)**. For **(A)**-**(C)**, all samples were treated for 4 days post infiltration (dpi) under light or dark conditions. **(D)** Typical endocytosis (black arrow) and 'blebbing' structure (red arrow) of plastids in dark-incubated *SGR*-overexpressing leaf regions. Bar = 5 μm. **(E)** and **(F)** Plastid number per cell area **(E)** and cross-sectional area of individual plastids **(F)** measured in cells of Figure 5. Samples were collected from *SGR*- and *EYFP*-overexpressing leaves at 1, 2, and 3 dpi in the dark. At least 125 individual plastids and 18 cells from five independent leaf regions were measured. Data are means ± SE. Asterisks indicate significant differences between the SGR and EYFP samples (two-way ANOVA followed by Sidak's multiple comparisons test, *, $P < 0.05$, ****, $P < 0.0001$ or better).

Figure 7. Plastid differentiation in the SGR region is independent of carotenoid synthesis.

(A) Representative images of dark-incubated *SGR*- and *EYFP*-overexpressing leaves treated with NF and CPTA. **(B)** Representative images of plant leaf phenotype after NF and CPTA treatment. **(C)** Total carotenoid levels of dark-incubated *SGR*- and *EYFP*-overexpressing leaves treated with NF and CPTA. The pigment level is presented as the ratio of the total peak areas of carotenoids to that of the internal standard. Data are means ± SE ($n = 3$).

Figure 8. Postulated contribution of SGR to the regulation of plastid development.

In this model, the overexpression of SGR in dark-incubated N. benthamiana leaves modulates the chlorophylls/carotenoid ratio and induces the development from chloroplasts to the carotenoid-bearing plastids, which we propose to term as the "chromo-gerontoplast", because its further transition to chromoplasts in ripen fruits or gerontoplasts in senescent leaves is to be determined by a multitude of other developmental cues.

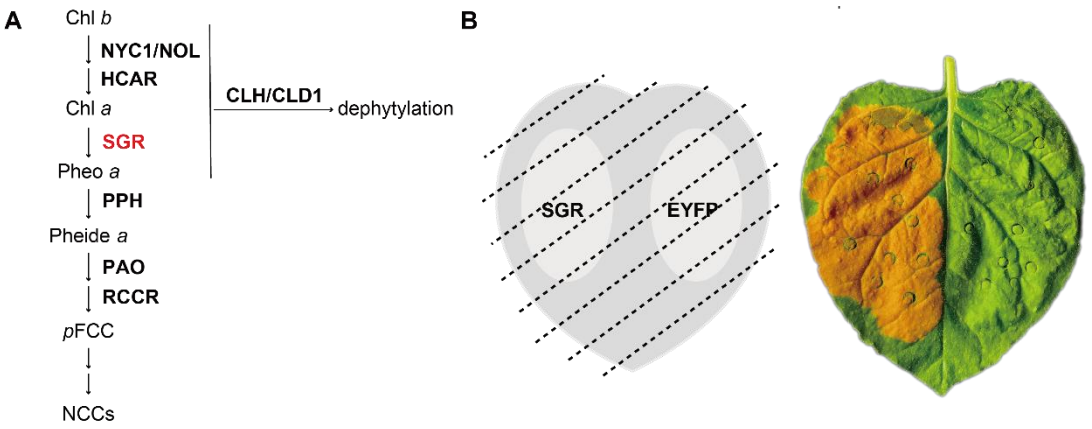

Figure 1. Transient overexpression of *SGR* in dark-incubated leaves transforms the color from green to bright orange.

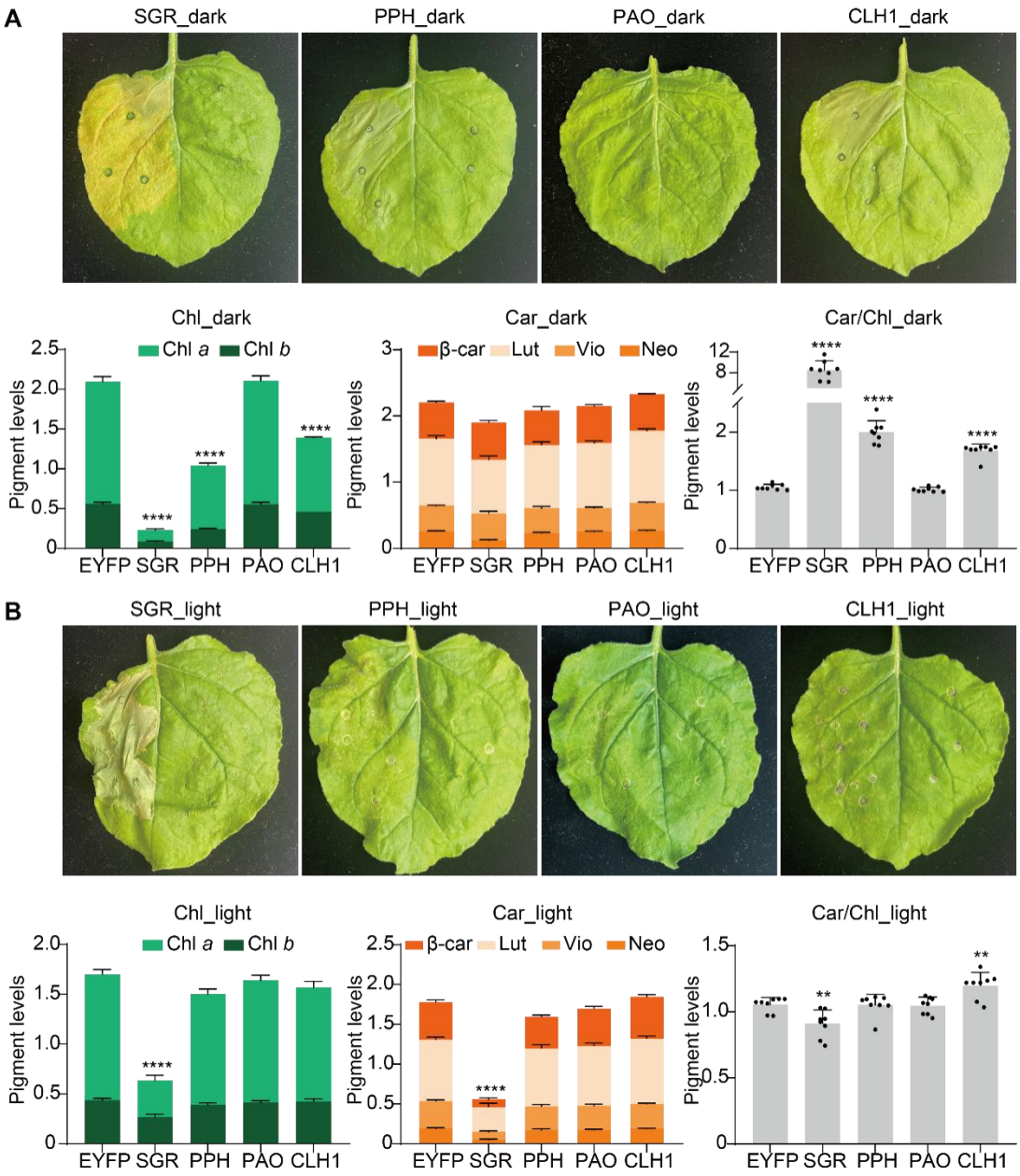

Figure 2. The overexpression of *SGR* leads to the most conspicuous alteration in the carotenoid-chlorophyll ratio.

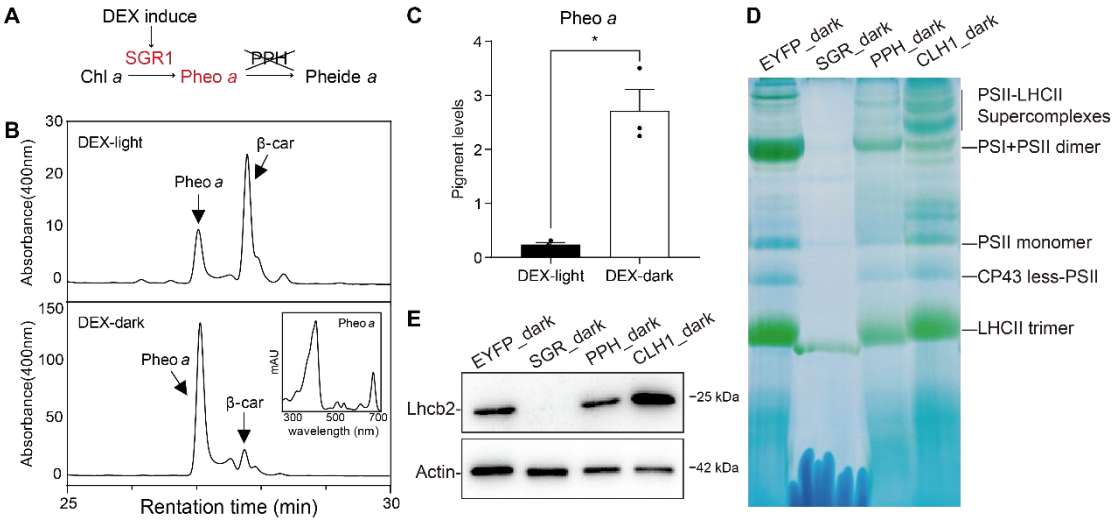

Figure 3. SGR disassembles the photosynthetic complexes by initiating the overall degradation of chlorophylls in darkness.

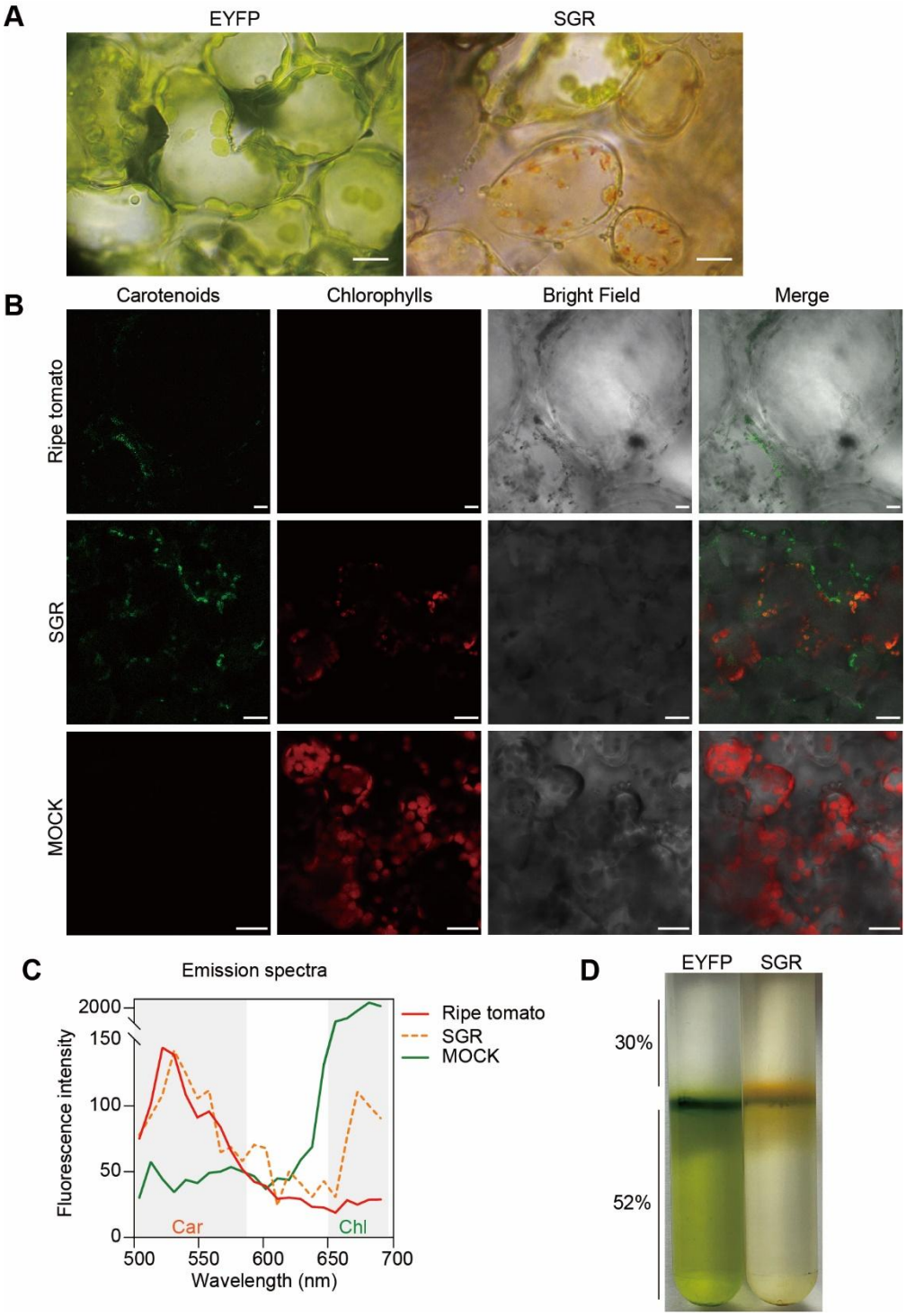

Figure 4. Plastids in orange SGR-region show carotenoid-bearing structures.

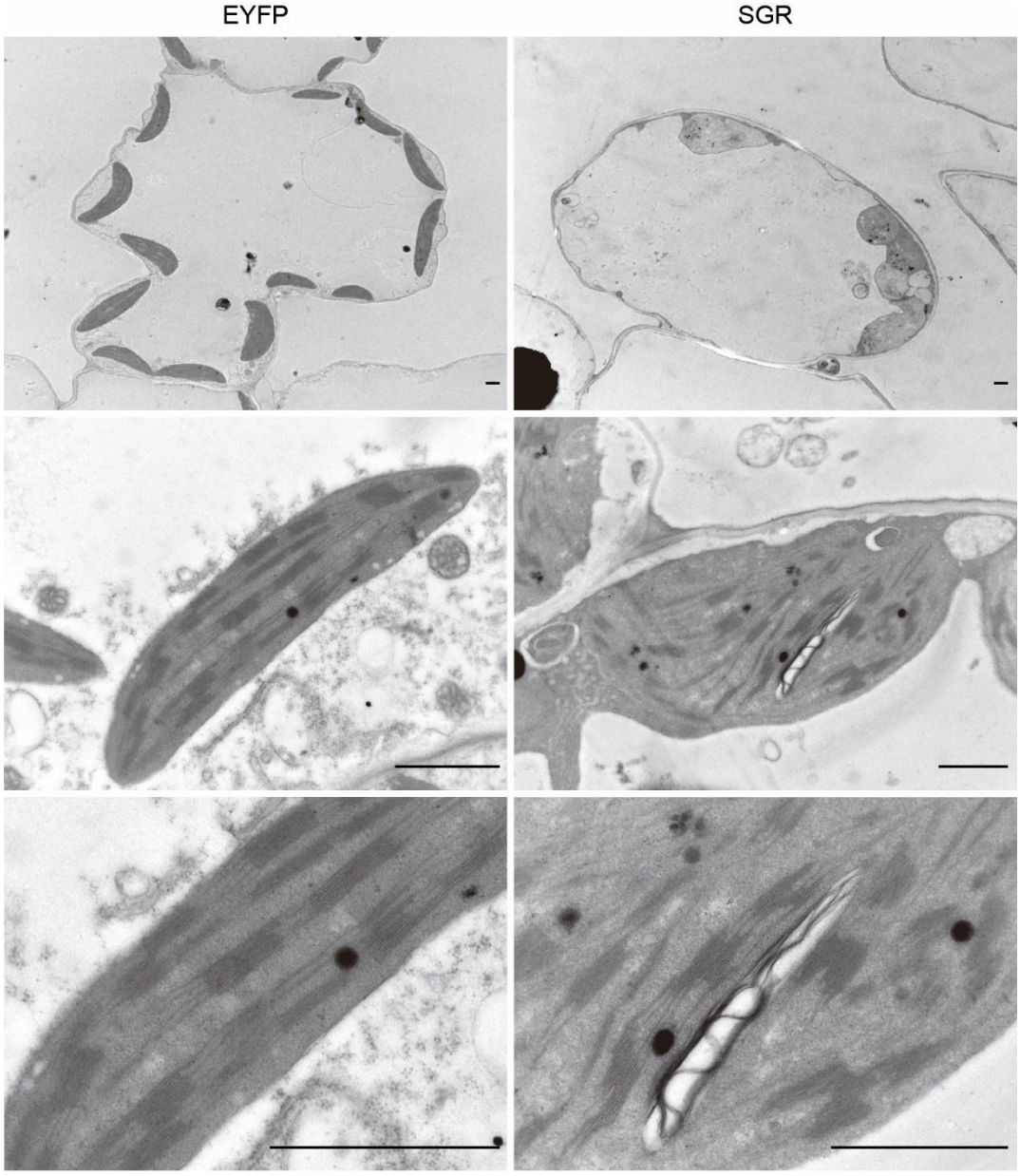

Figure 5. Electron micrographs of mesophyll cell plastids of dark-incubated *N. benthamiana* leaves overexpressing *SGR* and *EYFP*.

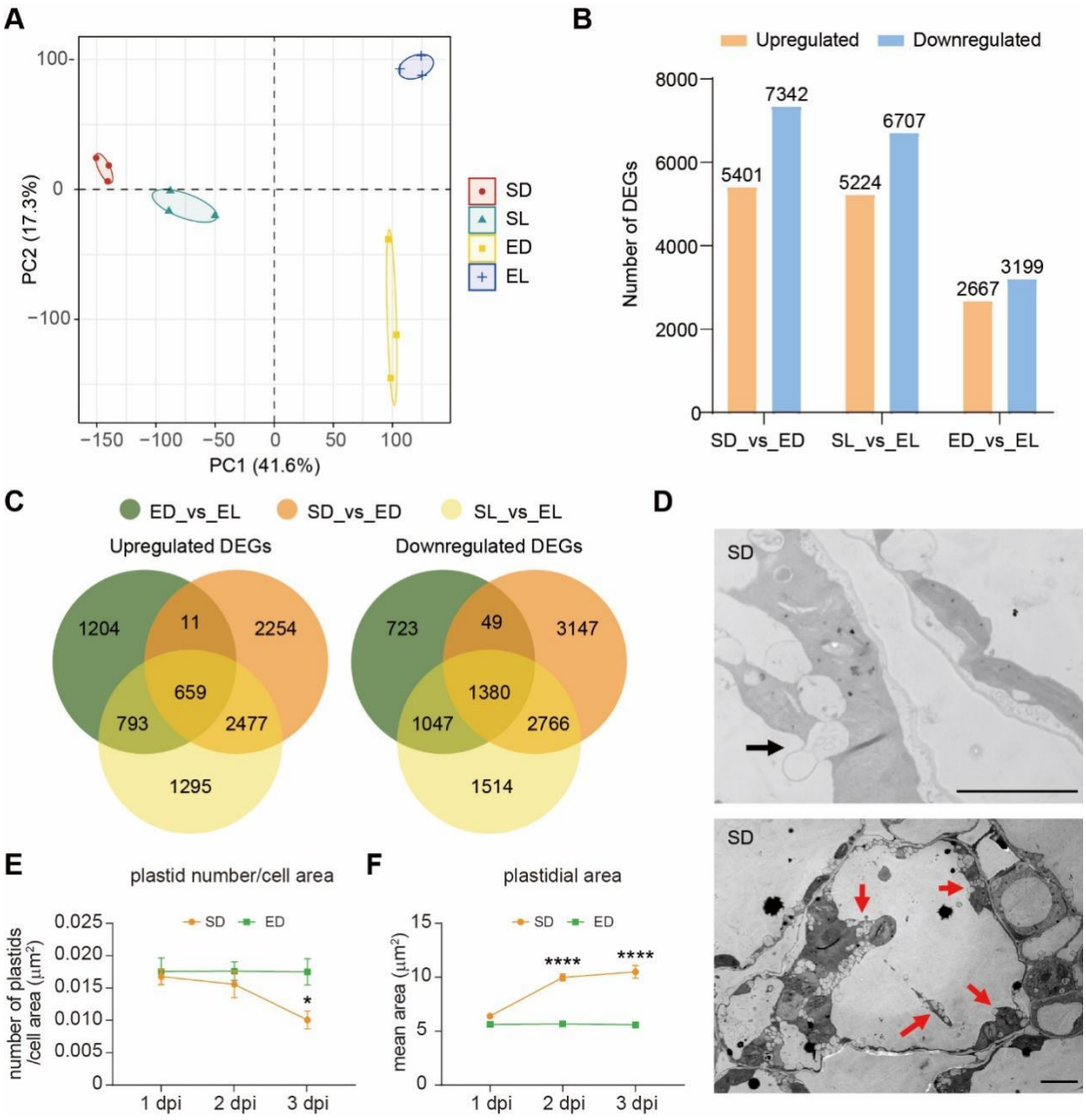

Figure 6. Transcriptomic analysis of *SGR*-induced gene expression.

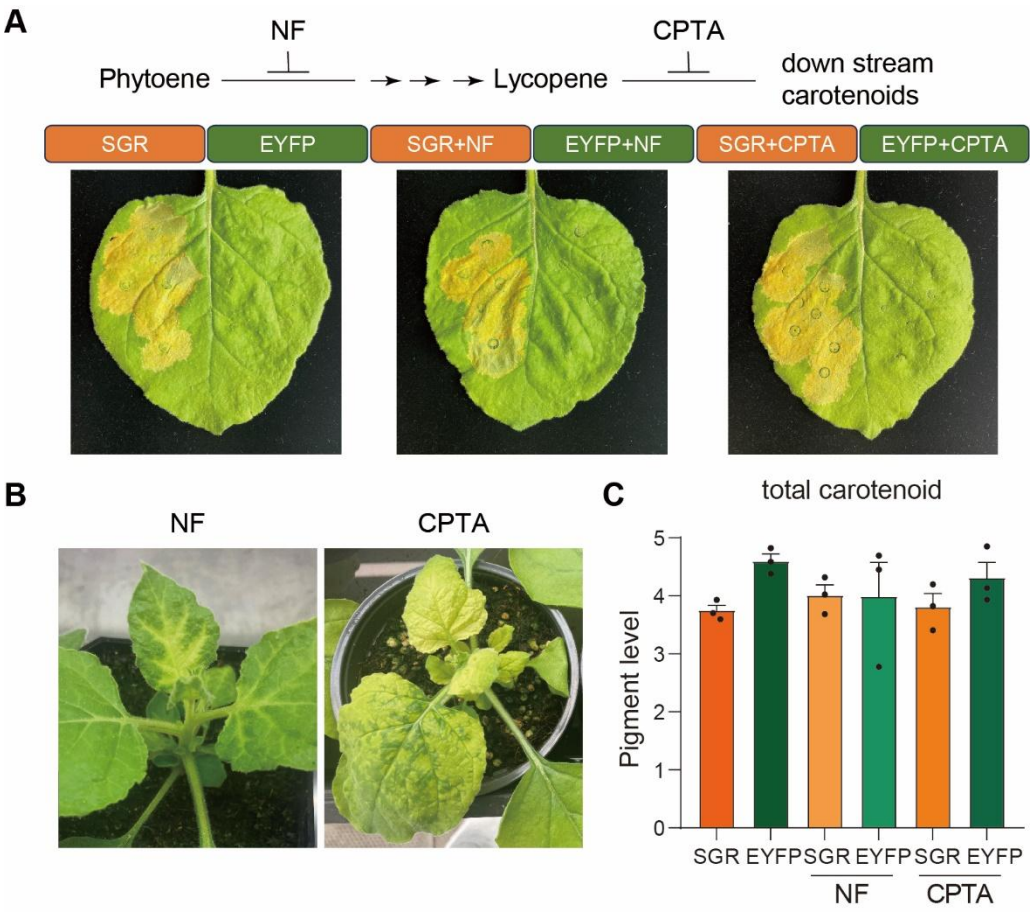

Figure 7. Plastid differentiation in the SGR region is independent of carotenoid synthesis.

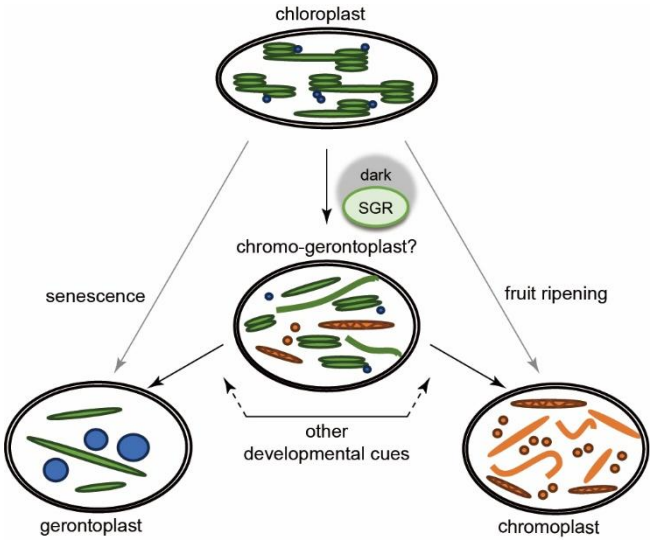

980 **Figure 8. Postulated contribution of *SGR* to the regulation of plastid development.**